boundary conditions be satisfied. Nevertheless, the agreement between these resonance frequencies and the observed ones strongly suggests that what we have observed in the simulation is a transient, which persists for a time $\tau \simeq \int_0^x dx/v_g$ before being wiped out by the reflection from $x = 0$. The critical shear length of this transient scales as $(L_s/L_n)_{\text{crit}} \simeq 10(m_i/m_e)^{1/4}$. Below it, the system is dominated by local fluctuations.

For comparison, frequencies of the two lowest previously predicted eigenmodes,[6] satisfying $\int_0^{P(\text{or } E)} Q^{1/2} dx = (l + \frac{1}{2})\pi/2$, are shown in Table II. Clearly, oscillations of the odd ($l = 1$) modes, which satisfy the imposed boundary condition $\varphi(0) = 0$ and are allowable in our system, are not the dominant feature of the spectra. In addition, we have carried out simulations which allow even ($l = 0$) modes by moving the rational surface to the middle of the system. Again, these eigenmodes were not observed. It is possible that the normal-mode oscillations take a longer time to be established and are masked by the unstable drift-wave transients described above.

The authors wish to thank Dr. C. Oberman, Dr. W. M. Tang, and Dr. G. Rewoldt for useful discussions.

This work was supported by the U. S. Department of Energy Contract No. EY-76-C-02-3073.

[1]P. H. Rutherford and E. A. Frieman, Phys. Fluids 10, 1007 (1967).
[2]L. D. Pearlstein and H. L. Berk, Phys. Rev. Lett. 23, 220 (1969).
[3]D. W. Ross and S. M. Mahajan, Phys. Rev. Lett. 40, 324 (1978).
[4]K. T. Tsang, P. J. Catto, J. C. Whitson, and J. Smith, Phys. Rev. Lett. 40, 327 (1978).
[5]T. M. Antonsen, Jr., Phys. Rev. Lett. 41, 33 (1978).
[6]L. Chen, P. N. Guzdar, R. B. White, P. K. Kaw, and C. Oberman, Phys. Rev. Lett. 41, 649, 913(E) (1978).
[7]W. W. Lee and H. Okuda, Phys. Rev. Lett. 36, 870 (1976).
[8]W. W. Lee, Y. Y. Kuo, and H. Okuda, Phys. Fluids 24, 617 (1978).
[9]E. Mazzucato, Phys. Rev. Lett. 36, 792 (1976).
[10]C. M. Surko and R. G. Slusher, Phys. Rev. Lett. 37, 1747 (1976), and 38, 258(E) (1977).
[11]W. W. Lee and H. Okuda, J. Comput. Phys. 26, 139 (1978).
[12]B. D. Fried and S. D. Conte, *The Plasma Dispersion Function* (Academic, New York, 1961).
[13]A. Kent and J. B. Taylor, Phys. Fluids 12, 209 (1969).
[14]R. B. White, J. Comput. Phys., to be published.

Long-Pulse Laser-Plasma Interactions at 10^{12}–10^{15} W/cm^2

B. H. Ripin, R. R. Whitlock, F. C. Young, S. P. Obenschain,[a] E. A. McLean, and R. Decoste[a]
Naval Research Laboratory, Washington, D. C. 20375
(Received 5 February 1979)

Laser-plasma interaction physics including absorption, plasma formation, heating, plasma expansion, and energy transport, are examined for 3-nsec Nd-laser irradiances between 10^{12} and 10^{15} W/cm^2. Efficient energy deposition and conditions favorable to ablative acceleration are found at 10^{12}–10^{13} W/cm^2, whereas reduced absorption, hot electrons, and fast ions are seen at 7×10^{14} W/cm^2. Suitability of the observed physics to pellet fusion is discussed.

Laser fusion experiments with long-pulse low-irradiance 1.06-μm laser pulses have been initiated[1] to study the interaction physics and ablative acceleration of thin foil targets under conditions which avoid the undesirable physics of short-pulse high-irradiance (< 1 nsec, $\gtrsim 10^{15}$ W/cm^2) interaction.[2,3] These unwanted effects at high irradiance include reduced light absorption due to the Brillouin backscatter instability, energetic electrons (tens of keV), high-energy ions that do not couple momentum efficiently to an imploding pellet, and inhibited thermal conductivity which reduce hydrodynamic efficiency and increase the symmetry requirements of the irradiation for laser-pellet fusion.

In contrast, Nd-laser–plasma experiments reported here at low irradiance (10^{12}–10^{13} W/cm^2) with 3-nsec pulses show efficient light absorption (80–90%), thermal electron distributions, near-classical heat transport, and hydrodynamically efficient ablativelike ion blowoff. At the somewhat higher irradiance of 7×10^{14} W/cm^2 the above-mentioned undesirable effects are once again observed. Long, low-irradiance pulses are therefore an interesting approach to laser fusion if the pellet shell can be accelerated stably. Particle-beam approaches to inertial confinement fusion are also in this same irradiance and

pulse-length regime, and it is anticipated that much of the physics involved in the present study will be applicable. The interaction physics is reported in this Letter and studies of the ablative acceleration appear elsewhere.[1,4] Also discussed herein are heat-flow measurements and their relationship to laser-beam uniformity requirements for successful implosion of pellets.

The experimental arrangement is discussed in detail in Ref. 1. Planar thin-foil targets of polystyrene (CH) or aluminum are mounted near the focal region of a 1-m aspheric $f/10$ lens at 6° from normal incidence. The target is tilted so that specular reflection can be distinguished from direct backscatter and so that the axis of symmetry of the plasma blowoff is discernible. The incident-beam irradiance is adjusted in these experiments by varying the position of the target between the lens and its focal point. The spatial and temporal laser-intensity distributions are both measured over four decades on each shot. A uniform intensity profile is important for ablative acceleration and Rayleigh-Taylor–stability experiments. Some effects of nonuniform illumination will be discussed.

Absorption.—Scattered light and total absorption measurements are made with use of a nearly 4π-sr box calorimeter[5] or an array of minicalorimeter pairs surrounding the target. To measure scattered light the box calorimeter is used with a Pyrex plasma shield.[1]

The box calorimeter measures the total absorbed light to be (85± 10)% of the incident light at 1×10^{13} W/cm^2 and (53± 10)% at 7×10^{14} W/cm^2. This agrees with other determinations.[6] The 16-μm-thick CH foil (apparently) goes underdense at 7×10^{14} W/cm^2 and transmission accounts for 15% of the incident energy. All the incident energy (± 10%) is accounted for when the Pyrex plasma shield is removed from the box calorimeter. Figure 1 shows three angular distributions of scattered light and plasma energy obtained with the minicalorimeter array. (X-ray and uv emission for CH targets is $<1\%$ of the incident energy and is neglected.) One notes the following general features: (1) Integration of both the scattered-light and particle-energy angular distributions are in agreement with the box-calorimeter results and with total energy balance. (2) The scattered-light intensity peaks towards the focusing lens and at the specular angle. The backscattered portion, primarily due to Brillouin backscatter, increases rapidly with irradiance above 10^{13} W/cm^2 in agreement with measurements with laser

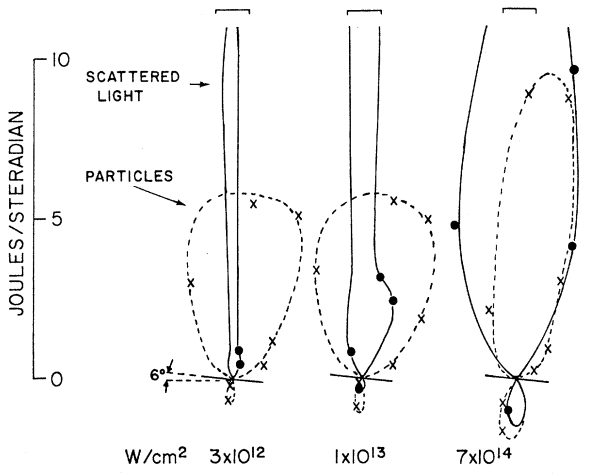

FIG. 1. Angular distributions of scattered light and plasma blowoff energy at three irradiances. Incident energies, focal-spot diameters, and CH target thickness were, respectively, 10.7 J, 450 μm, 10 μm; 15.3 J, 230 μm, 16 μm; and 16.1 J, 35 μm, 16 μm. Laser light is incident vertically from the top through the solid angles represented by bars.

pulses shorter than 1 nsec.[7] (3) The plasma blowoff peaks normal to the target.

Plasma formation and expansion.—For a peak laser irradiance of 2×10^{13} W/cm^2, plasma on the laser side of a 7-μm-thick Al target is first observed (interferometrically with a ~400-psec, 5320-Å probe pulse) 8 nsec prior to the peak of the laser pulse corresponding to an irradiance of $\approx 6\times 10^{9}$ W/cm^2. Initially the 10^{18} cm^{-3} density surface expands with a velocity normal to the target of 6.7×10^{6} cm/sec until 2 nsec before the laser pulse peak (20% of peak intensity), then speeds up to 3.5×10^{7} cm/sec and remains constant through the peak of the pulse. This latter velocity is approximately the average asymptotic ion ablation velocity measured with a time-of-flight charge collector array remote (25 cm) from the target.[1,4,8] A single ablation-velocity peak is observed at 10^{12}–10^{13} W/cm^2 whereas a second, energetic, ion component[1,2,9] appears at 7×10^{14} W/cm^2.

Electron temperature.—X-ray measurements imply information about the electron energy distribution and heat-flow properties in the absorption region and target interior. Bremsstrahlung continuum measurements from 1–50 keV are obtained with an array of eleven filtered detectors located at 120° to the incident laser direction. Time-integrated x-ray spectra for CH targets are shown in Fig. 2(a) for three irradiances.

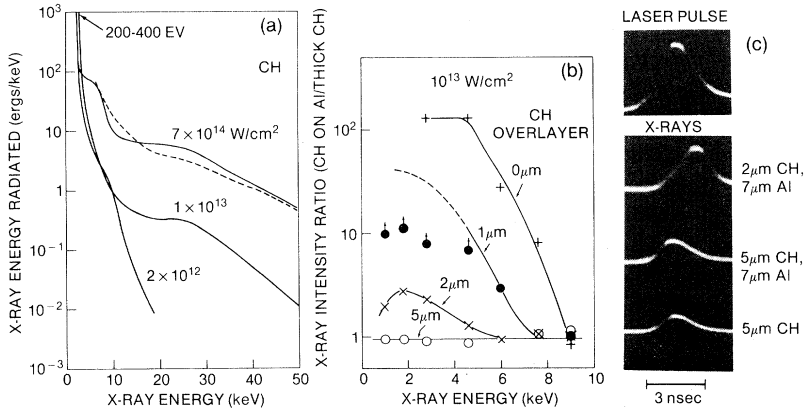

FIG. 2. (a) X-ray spectra measured with CH foil targets. Dashed spectrum is for 5×10^{15} W/cm^2, 5-J, 75-psec pulse. (b) X-ray intensity ratios for layered targets at x-ray energies from 1 to 9 keV. The data below 5 keV for a 1-μm-thick CH overlayer correspond to lower limits due to saturation of the detector amplifiers. (c) A temporal comparison of the emission of 1–2 keV x rays and the incident laser pulse ($\sim 10^{13}$ W/cm^2) for different layered targets. Amplitude scales are the same for all three x-ray traces.

Electron temperatures of 200–400 eV for both CH and Al targets are deduced from the lower-energy end of the spectra.[1] At 7×10^{14} W/cm^2, a much higher temperature (10–15 keV) is apparent in the high-energy tail of the spectra. The less-intense, high-energy tail at 10^{13} W/cm^2 may be caused by higher-irradiance hot spots on the beam. These energetic x-ray (and hence electron) tails, observed previously in similar experiments,[9] are thought to be due to electron tail heating.[10] The fast ion component appearing at 7×10^{14} W/cm^2 also suggests the onset of an energetic electron component at the higher irradiance.[2]

Axial heat flow.—An estimate of the depth of penetration of heat axially into the target is obtained by measuring the Al x rays from an Al target with a thin overcoating of CH.[3] The x-ray emission increases when the heat reaches the Al substrate due to its much higher x-ray emissivity (1–9 keV). X-ray intensities, normalized to pure CH, for several CH-overlayer thicknesses at 10^{13} W/cm^2 are shown in Fig. 2(b). Only minimal heating of the 7-μm Al substrate is apparent for a 2-μm CH overlayer and no heating of the substrate is evident for 3.5-, 4.0-, and 5.0-μm overlayers. The temporal x-ray emission into the 1–2 keV range, obtained with a 0.4-nsec risetime p-i-n diode with a 1-mil Be filter, is compared with the incident laser pulse in Fig. 2(c). These measurements are made on separate shots with use of the same p-i-n diode and oscilloscope (± 0.25 nsec jitter). A decrease in overlayer thickness from 5 to 2 μm causes the x-ray intensity to increase [consistent with Fig. 2(b)] and to be delayed relative to the laser pulse. The delayed emission indicates that the heat reaches the Al substrate well after the peak of the laser pulse. A similar behavior of x-ray emission is observed at 2×10^{12} W/cm^2 when the CH is reduced from 1.2 to 0.6 μm. Ablation depths inferred with use of the layered-target technique are consistent with mass accounting determinations.[4]

Lateral heat flow.—Lateral heat flow acts both as a heat loss mechanism from the interaction region and can prevent hot spots on the incident beam from producing uneven target acceleration and triggering hydrodynamic instabilities.

A suggestion that the lateral heat flow is not sufficient to eliminate the effects of laser intensity variations, at least in the region of 1-keV x-ray emission (a few times n_c)[11,12] is seen in Fig. 3. Here laser focal distributions are compared with constant-density contours from x ray pinhole photographs of the rear of (optically thin) CH foil targets. Intensity lobes are deliberately introduced into the focal distribution by placing varying widths of an opaque strip across the center of the focusing lens (a crude coded aperture). Note that the intensity variations (3:1) of the laser focal spot correlate well with those in the x-ray photograph (2:1).[13] Ignoring possible density profile perturbations this implies a temperature differential of ≈25%, i.e., 75 eV. This temperature differential is consistent with classical heat conductivity,[14] given the size of the laser beam nonuniformities and the plasma temperature inferred from x-ray measurements. Nonetheless, the heat flow is not sufficient to wash out lateral temperature gradients near the critical density

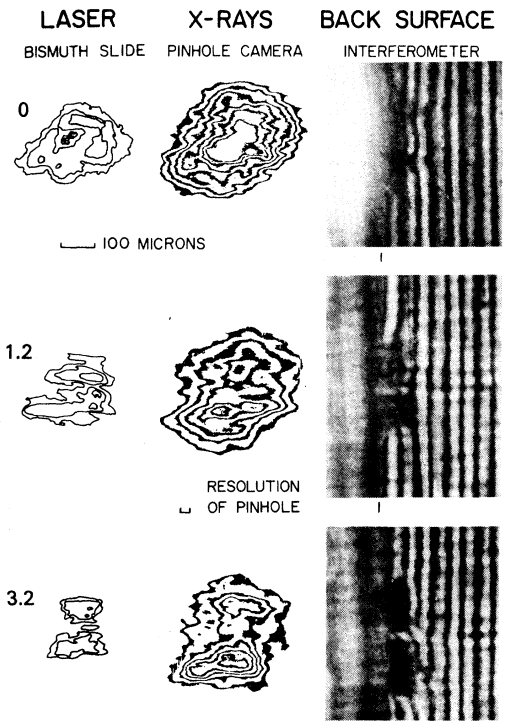

FIG. 3. Effect of beam nonuniformity on x-ray emission and ablation regions at 10^{13} W/cm^2. Left, laser focal-spot distributions; middle, constant-density contours of x-ray pinhole photographs of target rear; right, protrusions on target rear surface seen via interferometry. Numbers on left are the strip widths (in centimeters) placed horizontally across the lens diameter (8 cm) used to produce the spatially modulated focal spots.

due to gross (3:1) beam nonuniformities involving scale lengths greater than 30 μm.

However, the more important question is whether these nonuniformities are transmitted to the ablation surface (and thus to the accelerating target). This is demonstrated to be true, for gross nonuniformities, by comparing protrusions on the rear of the foil in Fig. 3 (observed by optical interferometry) to the intensity lobes introduced onto the incident beam profile. Other indications that lateral heat flow is low for our conditions are that the width of the ablatively accelerated portion of the target, observed interferometrically and via a Doppler-shift technique, remains approximately the size of the focal diameter.[1,4]

We have shown here that for long, low-irradiance, 1.06-μm laser pulses (2×10^{12}–1×10^{13} W/cm^2, 3 nsec) the absorption process is very efficient (> 80%) with minimal Brillouin backscatter and nonthermal electron heating. Low electron temperatures and good axial heat transport yield ion ablation velocities well suited for efficient acceleration of laser fusion pellet shells. This low-irradiance regime therefore has many characteristics favorable to laser fusion. Hot regions in the x-ray emission, due to corresponding nonuniformities in the focal-spot distribution, suggest that lateral heat flow is low but near classical. As a consequence, gross beam nonuniformities are transmitted to the ablation surface.

Contributions from the following to this work are appreciated: S. E. Bodner, J. A. Stamper, J. Grun, P. Moffa, S. Gitomer, J. Boris, S. H. Gold, M. Fink, N. Nocerino, E. Turbyfill, C. M. Dozier, and J. W. Criss. This work was supported by the U. S. Department of Energy.

[a]Present association: Sachs-Freeman Association, Bladensburg, Md.

[1]Naval Research Laboratory Laser-Plasma Interaction Group Report No. 3890, 1978, edited by B. H. Ripin (unpublished); B. H. Ripin *et al.*, to be published.

[2]B. H. Ripin *et al.*, Phys. Rev. Lett. 39, 611 (1977); R. Decoste and B. H. Ripin, Phys. Rev. Lett. 40, 34 (1978); D. W. Phillion, W. L. Kruer, and V. C. Rupert, Phys. Rev. Lett. 39, 1529 (1977); E. K. Storm *et al.*, Phys. Rev. Lett. 40, 1570 (1978).

[3]F. C. Young *et al.*, Appl. Phys. Lett. 30, 45 (1977); B. Yaakobi and T. C. Bristow, Phys. Rev. Lett. 38, 350 (1977); A. Zigler *et al.*, J. Phys. D 10, L159 (1977).

[4]R. Decoste *et al.*, Phys. Rev. Lett. 42, 1673 (1979).

[5]S. R. Gunn, Lawrence Livermore Laboratory Report No. UCID-17308, 1976 (unpublished); R. R. Whitlock, to be published.

[6]O. N. Krokhin *et al.*, Zh. Eksp. Teor. Fiz. 69, 206 (1975) [Sov. Phys. JETP 42, 107 (1976)]; J. P. Anthes *et al.*, Bull. Am. Phys. Soc. 23, 777 (1978).

[7]B. H. Ripin *et al.*, Phys. Rev. Lett. 33, 634 (1974).

[8]J. P. Anthes, M. A. Gusinow, and M. K. Matzen, Phys. Rev. Lett. 41, 1300 (1978); M. A. Gusinow *et al.* Appl. Phys. Lett. 33, 800 (1978); M. K. Matzen and R. L. Morse, Phys. Fluids 22, 654 (1979).

[9]N. G. Basov *et al.*, Elektron. 5, 126 (1973) [Sov. J. Quant. Electron. 3, 444 (1974)]; R. A. Haas *et al.*, Phys. Rev. Lett. 39, 1533 (1977); J. S. Pearlman and J. P. Anthes, Appl. Phys. Lett. 27, 581 (1975).

[10]C. M. Armstrong *et al.*, Naval Research Laboratory Report No. 3829, 1978 (to be published).

[11]B. H. Ripin *et al.*, Phys. Rev. Lett. 34, 1313 (1975).

[12]P. J. Moffa, J. H. Orens, and J. P. Boris, to be published.

[13]Similar hot spots were observed above 10^{14} W/cm^2 in x-ray pinhole photographs taken of the front side of a target in H. D. Shay *et al.*, Phys. Fluids 21, 1634 (1978).

[14]L. Spitzer, *Physics of Fully Ionized Gases* (Wiley, New York, 1961).

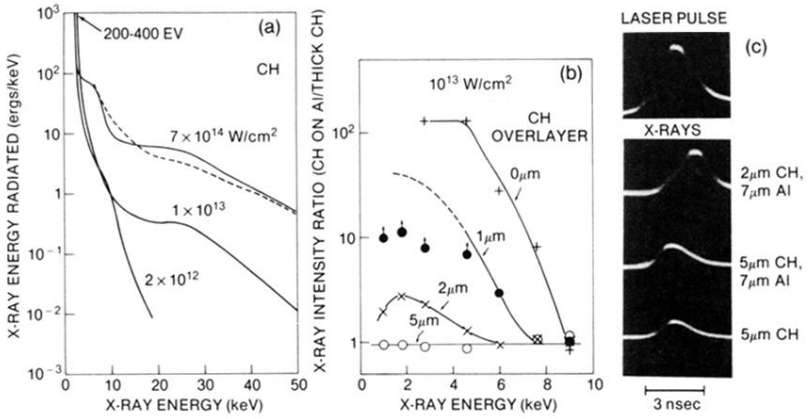

FIG. 2. (a) X-ray spectra measured with CH foil targets. Dashed spectrum is for 5×10^{15} W/cm^2, 5-J, 75-psec pulse. (b) X-ray intensity ratios for layered targets at x-ray energies from 1 to 9 keV. The data below 5 keV for a 1-μm-thick CH overlayer correspond to lower limits due to saturation of the detector amplifiers. (c) A temporal comparison of the emission of 1–2 keV x rays and the incident laser pulse ($\sim 10^{13}$ W/cm^2) for different layered targets. Amplitude scales are the same for all three x-ray traces.

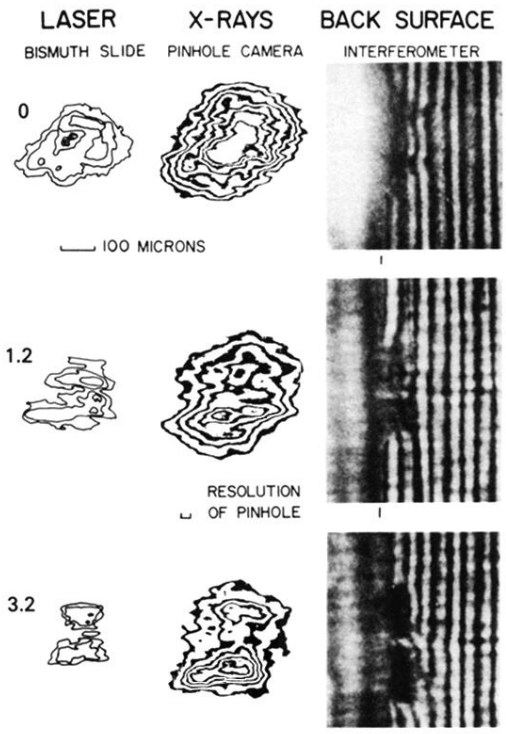

FIG. 3. Effect of beam nonuniformity on x-ray emission and ablation regions at 10^{13} W/cm^2. Left, laser focal-spot distributions; middle, constant-density contours of x-ray pinhole photographs of target rear; right, protrusions on target rear surface seen via interferometry. Numbers on left are the strip widths (in centimeters) placed horizontally across the lens diameter (8 cm) used to produce the spatially modulated focal spots.